ACS APPLIED MATERIALS & INTERFACES

Research Article

Cite This: ACS Appl. Mater. Interfaces 2019, 11, 44682−44690

www.acsami.org

Wettability Control in Tree Structure-Based 1D Fiber Assemblies for Moisture Wicking Functionality

Ning Mao,[†] Hui Peng,[†] Zhenzhen Quan,[†,‡] Hongnan Zhang,[†] Dequn Wu,[†] Xiaohong Qin,[*,†] Rongwu Wang,[†] and Jianyong Yu[‡]

[†]Key Laboratory of Textile Science & Technology of Ministry of Education, College of Textiles and [‡]Innovation Center for Textile Science and Technology, Donghua University, Shanghai 201620, P.R. China

Supporting Information

ABSTRACT: One of the fundamental properties of natural systems is their water transport ability, and living systems have efficient moisture management features. Here, a unique structure, inspired by the water transfer behavior in trees, was designed for one-dimensional (1D) fiber assemblies. In this 1D fiber assembly structure, a differential capillary effect enabling rapid water transfer at the interface between traditional cotton fibers and electrospun nanofibers was explored. A tree-like structure yarn was constructed successfully by novel electrospinning technology, and the effect was quantitatively controlled by precisely regulating the fibers' wettability. Fabrics based on these tree-like core-spun yarns possessed advanced moisture-wicking performance, a high one-way transport index (R) of 1034.5%, and a desirable overall moisture management capability of 0.88, which are over two times higher than those of conventional fabrics. This moisture-wicking regime endowed these 1D fiber assemblies with unique water transfer channels, providing a new strategy for moisture-heat transmission, microfluidics, and biosensor applications.

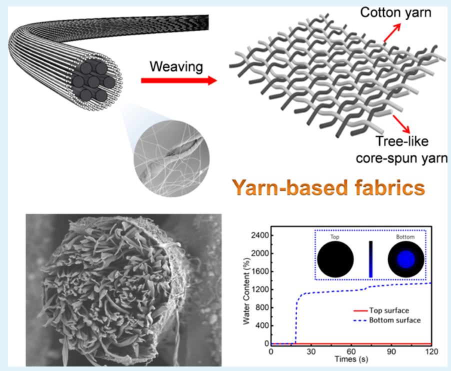

KEYWORDS: *tree-like structure, microfluidic flow, electrospun core-spun yarns, yarn structure, moisture-wicking function*

1. INTRODUCTION

Water transport ability is one of fundamental properties of engineering materials.[1] This property consistently plays an essential role in functional devices, such as biosensors,[2] artificial muscles,[3] and functional fabrics.[4] For these systems, the fluidic flow within them should generally be precisely controlled to successfully achieve the desired function. There are two effective strategies for enhancing moisture management: structural design and material optimization.

Nature has inspired materials engineering, and many novel structures have been derived from living systems, especially plants. In the area of water transport, tree-like structures, which are compositions with a scale gradient (e.g., from large pores to small pores, from the micrometer to the nanometer scale) in a specific direction, are a classic design.[5] Based on this theory, a biomimetic fabric consisting of three layers and constructing tree-shaped channel nets in the thickness direction was reported,[6,7] showing great liquid management performance. In addition to these traditional weaving fabrics, many nanofibrous membranes, in which water could be transported only from one side to another side, have been applied in directional fluid transport.[8] In the same way, these membranes usually contain many layers, and different layers are made of different fibers (different scales,[9,10] different surface energies[11−13]). For example, in a typical hierarchical structure,[14] where a Laplace pressure difference between different layers exists, the pressure difference provides the driving force for directional fluidic flow.[15−18]

Another useful method is material optimization, which constructs the surface energy gradient of materials to achieve directional water movement. One effective category is Janus wettability,[19] which means that the two sides of a fabric or membrane have completely different wettabilities. Depending on the surface modification technology, such as UV irradiation,[20,21] plasma treatment,[22] and electrospray,[23] Janus wettability could be realized successfully and simply. These Janus materials are usually based on the structures mentioned above, including traditional fabrics,[21−23] electrospun membranes,[24,25] and copper meshes.[26,27] Therefore, material optimization and structural design consistently work together to enhance the differential capillary effect. For example, in a composite three-dimensional (3D) fibrous membrane[28] that was composed of three layers, the fibers in each layer in the thickness direction tended to become finer, and at the same time, wettability of these layers became stronger. Thus, the inner pressure gradient could drive the rapid directional transport of water through the membrane.

Despite extensive progress in traditional fabrics and 3D fibrous membranes, materials engineering of tree-like structure

Received: August 12, 2019
Accepted: October 9, 2019
Published: October 9, 2019

DOI: 10.1021/acsami.9b14370
ACS Appl. Mater. Interfaces 2019, 11, 44682−44690

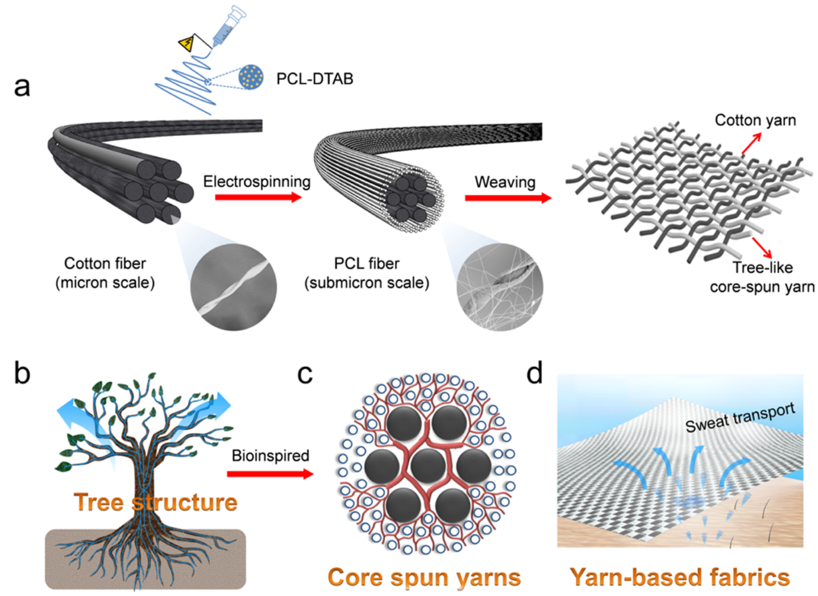

Figure 1. Design of the tree-like core-spun yarns. (a) Process of electrospinning to prepare tree-like core-spun yarns and fabrics. (b) Model diagram of water transport in a tree. (c) Schematic diagram of a tree-like core-spun yarn. The outer circles denote electrospun nanofibers, and the inner circles denote cotton fibers. (d) Schematic demonstration of the sweat transport process in core-spun yarn-based fabrics.

designs in one-dimensional (1D) fiber assemblies is still lacking. Although there are some research about wicking properties of electrospun nanofiber yarns,[29,30] wettability control by using electrospinning yarns was not realized. As electrospun yarn technology developed,[31,32] nanofibers could be collected in 1D shapes, and nanofiber properties could be optimized. Moreover, electrospun nanofiber yarns are attracting increasing attention because of their durability and flexibility for further processing, such as weaving and knitting, thereby demonstrating their numerous applications in moisture-heat transmission,[33] microfluidics,[34−36] tissue engineering,[37] and biosensors.[38]

Here, we demonstrate the controllable water transport performance in a 1D fiber assembly combining a tree-like structure design and material optimization. The tree structure was introduced into a 1D fibrous system, where cotton fiber was adapted as a framework and coated with electrospun polycaprolactone (PCL) nanofibers. In this yarn system, cross-section hierarchical channel structures were constructed by differential capillaries with multibranch microchannels and sub-microchannels. Furthermore, these tree-like core-spun yarns were engineered with precisely controlled surface wettability by a simple and effective method. Unlike the traditional fibrous membranes, these yarns could be fabricated into woven fabrics, demonstrating the possibility for further processing. As a result, such fabrics with differential capillary effects showed outstanding moisture management performance and a high one-way transport value, both of which were much superior to those of conventional fabrics. Finally, mathematical simulation of water flow within the fabrics confirmed that the water transfer behavior of tree-like core-spun yarns could be quantitatively controlled by regulating their surface wettability. Consequently, research on 1D fiber assemblies combining a tree-like structure design with surface wettability control provides wide application prospects in biosensors, artificial muscles, and moisture functional fabrics.

2. EXPERIMENTAL SECTION

2.1. Materials and Chemicals. PCL (Sigma-Aldrich, China, M_w = 80 000), chloroform (≥99%, Sigma-Aldrich, China, anhydrous), and methanol (≥99.8%, Sigma-Aldrich, China, anhydrous) were obtained. Absolute ethanol (C_2H_5OH), silicone oil, and eosin Y (water soluble) were purchased from Sinopharm Chemical Reagent Co., Ltd., China. Dodecyltrimethylammonium bromide (DTAB) (≥98%, Sigma-Aldrich, USA) was obtained. Commercial cotton yarns were purchased from Dongguan Zheng Yu Co., Ltd., China.

2.2. Preparation of Tree-like Yarns. A PCL solution was made by dissolving 1.04 g PCL in 9 mL of chloroform and 3 mL of methanol. DTAB was added to the PCL solution at concentrations of 0.25, 0.5, 1, 2, and 3 mg/mL. Tree-like yarns were fabricated through specialized technology for electrospun yarns.[31,32] Two oppositely spinning needles were placed symmetrically on the two sides of a metal disc and supplied with positive and negative voltages. During the electrospinning process, the commercial cotton yarn crossed through the rotating disc and electrospun nanofibers were coated on its surface. The specific parameters are as follows: the applied voltage was ±9.8 kV, the distance between the two needles was 20 cm, and the flow rate was 0.8 mL/h. The PCL, 0.25DTAB/PCL, 0.5DTAB/PCL, 1DTAB/PCL, 2DTAB/PCL, and 3DTAB/PCL core-spun yarns and the membranes used to test contact angles were prepared under the same conditions at a temperature of 23 ± 2 °C and a humidity of 50 ± 5%.

2.3. Preparation of Core-Spun Yarn-Based Fabrics. Tree-like yarns were introduced into a plain woven fabric by using a SGA598 semiautomatic small sample machine. The tree-like yarns were used as the weft yarns, and commercial cotton yarns were used as the warp yarns. The warp density was designed as 430/10 cm, and the weft density was 400/10 cm.

2.4. Morphological and Chemical Analysis of Tree-Like Yarns. The morphology of the tree-like yarns was observed by a DXS-10ACKT scanning electron microscope. Tree-like yarns were immersed in silicone oil to analyze the sheath−core structure with a polarizing microscope (LV100N POL, Nikon). Thermogravimetric analysis (TGA) was performed with a TGA 4000 (PerkinElmer Co., Ltd.) from 50 to 800 °C. Attenuated total reflection Fourier transform infrared (FTIR) spectra were recorded by a PerkinElmer Spectrum Two from 400 to 4000 cm^{-1}. Surface elemental analysis of polarized light DTAB/PCL nanofibers was performed with an X-ray photo-

DOI: 10.1021/acsami.9b14370
ACS Appl. Mater. Interfaces 2019, 11, 44682−44690

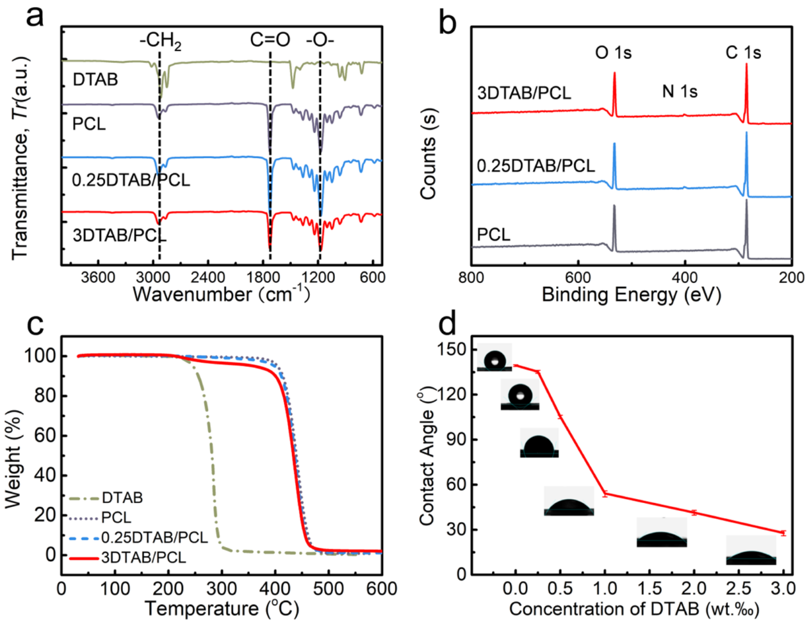

Figure 2. Wettability of PCL nanofibers. (a) FTIR spectra of DTAB powder and PCL, 0.25DTAB/PCL, and 3DTAB/PCL nanofibers. (b) XPS spectra of PCL, 0.25DTAB/PCL, and 3DTAB/PCL nanofibers. (c) TGA from 50 to 800 °C of DTAB powder and PCL, 0.25DTAB/PCL, and 3DTAB/PCL nanofibers. (d) Contact angles of PCL nanofiber membranes prepared with different DTAB concentrations.

electron spectrometer (XPS; Escalab 250Xi, Thermo Fisher Scientific Inc.)

2.5. Analysis of Water Transport Performance. Moisture management performance was tested by a moisture management test (MMT; SDLATLAS M290) with a testing liquid (9 g of NaCl added to 1 L of water with a conductivity of 16 ± 0.2 ms; AATCC TM 195). The MMT with two electrical sensors on the top and bottom side of samples could measure the resistance on the top and bottom surface of the fabrics, and these resistance values could be converted into the water content. Water contact angles (4 μL water droplet) were tested by a contact angle measurement apparatus (OCA15EC, GmbH). The wicking height was measured based on the AATCC TM 197 test method. The tree-like yarn-based fabrics were cut into strips (20 cm × 3 cm) along the weft direction (tree-like yarn). The water evaporation rate was characterized by a water evaporation rate tester (FFZ191, Wenzhou Fang Yuan Co., Ltd., China), where a sample (10 cm × 10 cm) was wetted with 0.2 g of deionized water and the weight change was recorded every 5 minutes. Water spreading behavior on the fabric surface was characterized by an infrared (IR) thermal camera (Fotric 220s). A water droplet (4 °C, 50 μL) was dropped onto the sample (2 cm × 2 cm, 25 °C, room temperature), and the water motion was recorded. Fluorescence images were acquired by a microscopy system (Ti−S, Nikon Corporation), and eosin Y (water soluble) was used to label the wetted regions within the tree-like yarns.

3. RESULTS AND DISCUSSION

3.1. Design of the Tree-Like Core-Spun Yarns. In tree-like core-spun yarns, cotton is a natural hydrophilic material that readily absorbs a large amount of water but has difficulty in driving the water out, while PCL is a human-made material with low moisture recovery (0.4%) and could be designed to achieve appropriate wettability, enabling quick water transfer and low water absorption. Theoretically, for 1D fiber assemblies, water transport behavior is mainly governed by the capillary pressure p, which can be defined by eq 1

$$p = \frac{2\gamma \cdot \cos\theta}{\overline{r}} \tag{1}$$

where γ is the liquid surface tension, θ is the contact angle of the fiber, and $\overline{r}$ is the capillary equivalent radius of the capillaries.

Tree-like core-spun yarns were fabricated by electrospinning technology, as shown in Figures 1a and S1. Nanofibers, electrospun by two opposite needles, were collected by a metal disc in an aligned way. During this process, commercial cotton yarns (black) went through the device so that they would be coated with nanofibers. This process was continuous, and the production reached an effective rate of 2 m/min. Water inside these yarns could be completely pushed out because of numerous submicron channels constructed by nanofibers in the outer layer, which is similar to water moving from the root to the leaf veins in plants (Figure 1b,c). To characterize their water transport performance, core-spun yarn-based fabrics were woven, which strengthened their differential capillary and push−pull effects. Based on the differential capillary pressure caused by the scale difference between the nanofibers in the shell layer and the cotton fibers in the core layer, liquid water can be transferred from the side touching the skin through the interface between two layers and finally to another side exposed to the environment (Figure 1d).

3.2. Morphology and Properties of Tree-Like Core-Spun Yarns. PCL nanofibers with different surface wettabilities were obtained from PCL solutions with DTAB concentrations ranging from 0 to 3 wt ‰. With increasing DTAB concentration, FTIR spectra (Figure 2a) of the PCL/DTAB nanofibers did not show obvious changes because the stretching vibrations of PCL covers the bands corresponding to DTAB, including the peaks at 2926 cm^{-1} for methylene $-CH_2$, 1723 cm^{-1} for carbonyl C═O stretching, and 1192 cm^{-1} for lactone−O−stretching. However, the surface chemical composition of the DTAB/PCL nanofiber layer, as assessed by XPS, showed a new characteristic peak of 3DTAB/PCL formed at 398 eV (N 1s), confirming the existence of DTAB on the nanofiber surface (Figure 2b). Furthermore, TGA was performed. As demonstrated by Figure 2c, the decomposition

DOI: 10.1021/acsami.9b14370
ACS Appl. Mater. Interfaces 2019, 11, 44682−44690

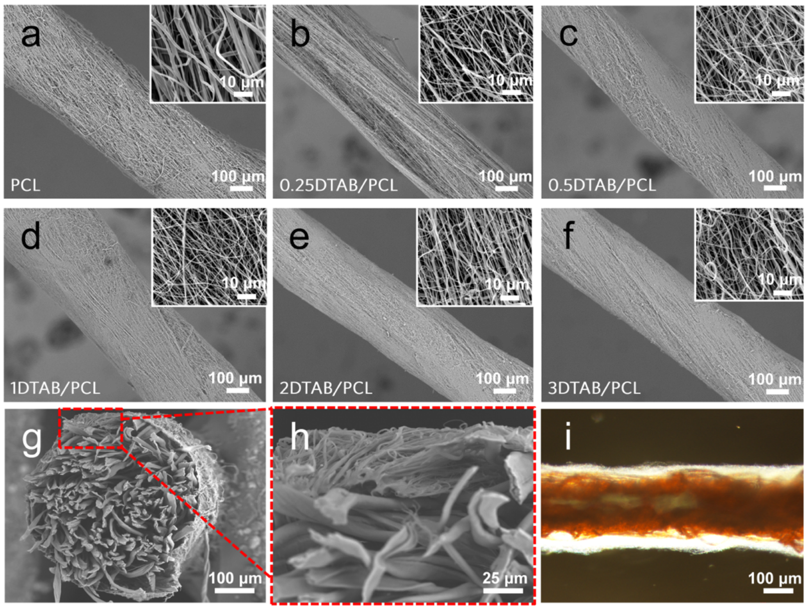

Figure 3. Surface morphology of tree-like yarns coated with (a) PCL, (b) 0.25DTAB/PCL, (c) 0.5DTAB/PCL, (d) 1DTAB/PCL, (e) 2DTAB/PCL, and (f) 3DTAB/PCL nanofibers. (g) Cross-section of a tree-like yarn, wherein the inner layer consists of cotton fibers and (h) the outer layer consists of nanofibers. (i) Polarized light optical microscopy images of tree-like yarn immersed in silicone oil, where the outer white part is the nanofiber layer and the inner red part is the cotton layer.

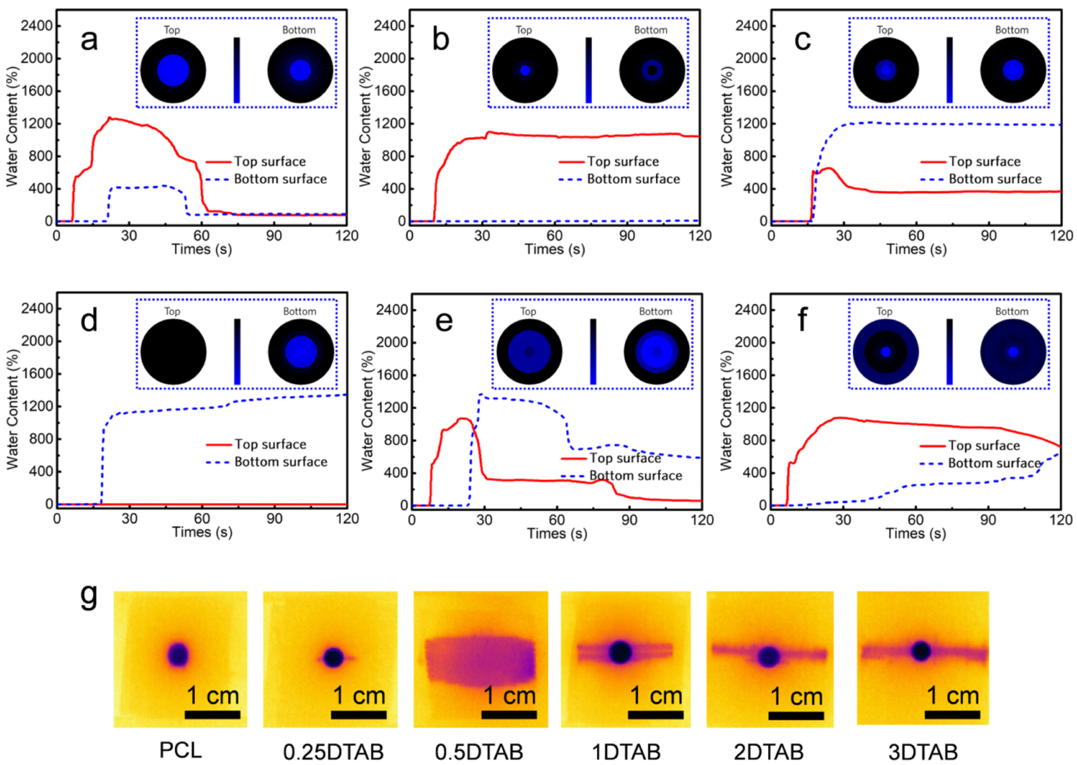

Figure 4. MMT results for tree-like core-spun yarn-based fabrics: (a) PCL fabric, (b) 0.25DTAB/PCL fabric, (c) 0.5DTAB/PCL fabric, (d) 1DTAB/PCL fabric, (e) 2DTAB/PCL fabric, and (f) 3DTAB/PCL fabric. (g) IR thermal images of a water droplet spreading on the surface of tree-like yarn-based fabrics.

temperature of DTAB is approximately 280 °C, while that of the PCL nanofibers is approximately 450 °C. Although the curve of the 0.25DTAB/PCL nanofibers is similar to that of pure PCL, the 3DTAB/PCL samples has two obvious thermal decomposition processes, showing the addition of DTAB. Consequently, as the DTAB concentration increased, the contact angles of the PCL nanofibers decreased from 135° to 22° (Figure 2d). The roughness of PCL, 0.25DTAB/PCL, 0.5DTAB/PCL, 1DTAB/PCL, 2DTAB/PCL, and 3DTAB/PCL membranes was computed (Supporting Information note 1), resulting in the surface roughness of 18.7, 38.2, 41.3, 39.6,

DOI: 10.1021/acsami.9b14370
ACS Appl. Mater. Interfaces 2019, 11, 44682−44690

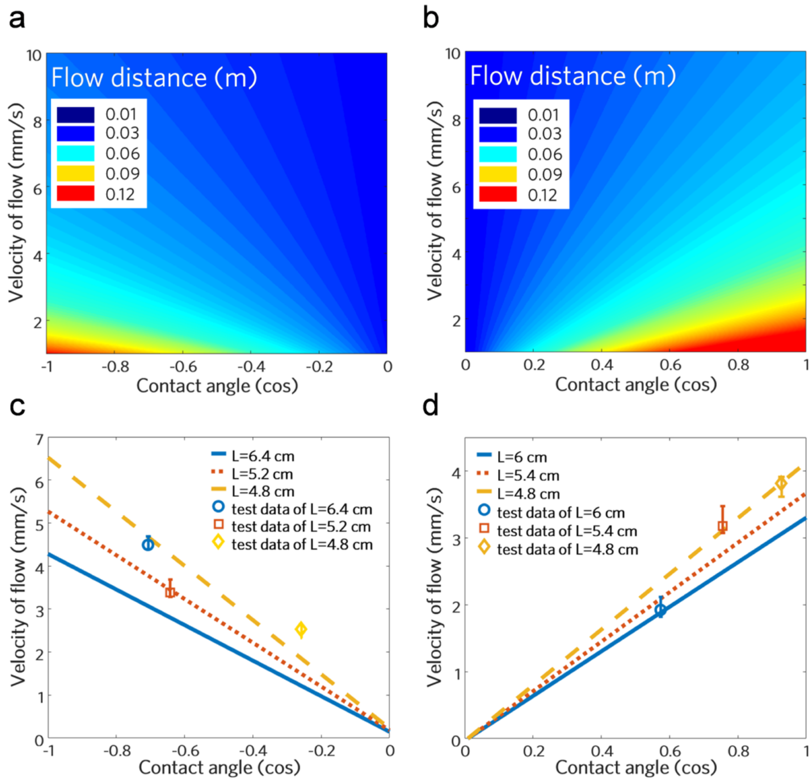

Figure 5. Simulation results of water moving on the surface of tree-like core-spun yarn-based fabrics, where (a) cos θ = [−1, 0] and (b) cos θ = [0, −1]. Flow velocity in the tree-like core-spun yarn-based fabrics as a function of the flow distance and contact angles, where (c) cos θ = [−1, 0] and (d) cos θ = [0, −1].

43.1, and 42.7, respectively. The wettability of PCL nanofibers should be precisely controlled.

Figure 3a−f shows the surface morphology of the core-spun yarns, indicating that the yarns were coated completely and PCL nanofibers were arranged in an aligned manner on the surface. Notably, the nanofibers in the pure PCL yarns were much thicker than those in the other yarns because the increase in the charge density of electrospinning solution induced by DTAB could strengthen the electric force and make the nanofibers thinner.[39,40] However, as the DTAB concentration in the PCL solution increased, the average diameter of the nanofibers, which was approximately 330 nm, did not noticeably change (Figure S2). Figure 3g,h shows cross-sectional scanning electron microscopy (SEM) images of a typical tree-like yarn, clarifying the tree-like structure and large scale difference between fibers in the outer layer (submicron scale) and those in the inner layer (micron scale). Specifically, the nanofibers in the sheath layer were approximately two orders of magnitude finer than the cotton fiber in the core layer, enabling a notable differential capillary effect. The sheath−core structure could be integrally observed by immersing the whole yarn into silicone oil (a liquid with a similar refractive index to PCL nanofibers); thus, the outer layer became transparent (Figure 3i). Based on this method, the thickness of the nanofiber layer was approximately 35 μm, and the sheath−core ratio was calculated as approximately 1:5.

3.3. Microfluidic Flow Control in Tree-Like Yarn-Based Fabric. To effectively analyze the microfluidic flow controlled by the tree-like core-spun yarns, the yarns were introduced into a typical plain woven fabric containing core-spun yarns in the weft direction and normal cotton yarns in the warp direction. A moisture management tester (MMT) was utilized to characterize the liquid flow state on the fabric surface and the fabric transport properties. For the PCL fabric (Figure 4a), the water content of the top surface (WCT) increased rapidly, and the wetting time of the top surface (WTT) was approximately 5.6 s, which was reflected by the horizontal intercept of the solid curve. When the WCT of the PCL fabric reached its highest value, the water content of the bottom surface (WCB) began to increase, and the wetting time of the bottom surface (WTB) was 20.1 s. This phenomenon indicated that water accumulated on the top surface only until it could transport from the top surface to the bottom surface; therefore, its one-way transport index was only −926%. For the 0.25DTAB/PCL fabric (Figure 4b), during the period when the WCT remained high, the bottom surface had no water content, which means that the microfluidic flow could not pass through the fabric. The reason why it was more difficult for water to pass through the 0.25DTAB/PCL fabric than the PCL fabric was that the DTAB concentration of 0.25 wt ‰ did not change the fibers' wettability obviously but did make their diameters much finer. According to eq 1, the negative capillary pressure (the direction is outwards) produced by these nanofibers should be enlarged, resisting water transport. As the wettability was increased continuously, control of the liquid flow became more effective (Figure 4c,d). In particular, the bottom surface of the 1DTAB/PCL fabric responded much more quickly than that of the other fabrics (the WTB was almost equal to the WTT). Moreover, water could transport through the 1DTAB/PCL fabric effectively, and its one-way transport index R reached 1034.5%. This high transport index value resulted from the negative pressure becoming positive when the contact angle of the nanofibers was less than 90°. However, when the contact angles of the nanofibers became

DOI: 10.1021/acsami.9b14370
ACS Appl. Mater. Interfaces 2019, 11, 44682−44690

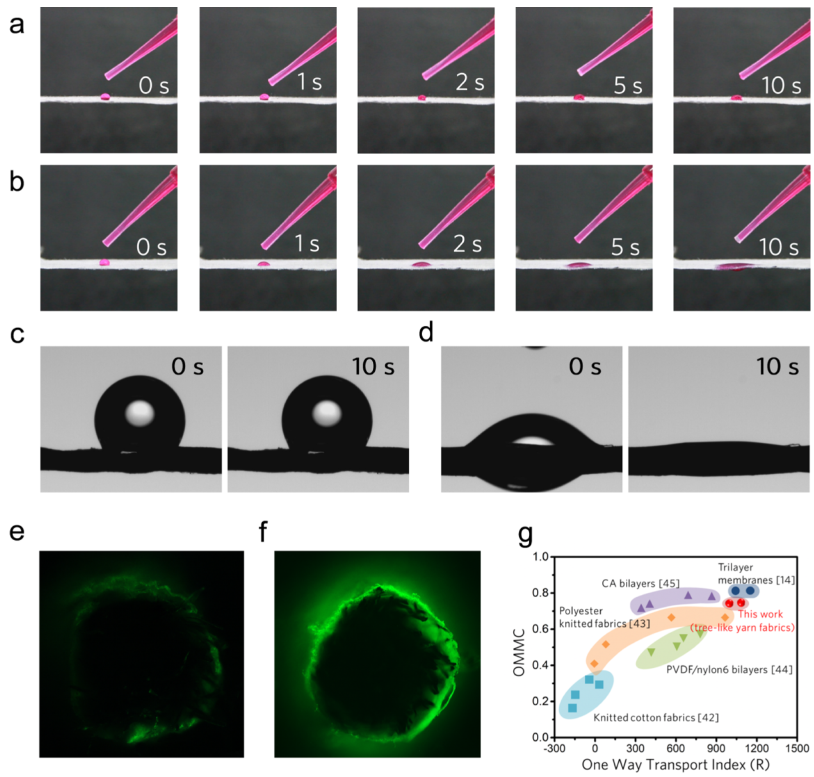

Figure 6. Water droplets spread on and penetrating through (a) the PCL core-spun yarn-based fabric and (b) the 1DTAB/PCL core-spun yarn-based fabric. Water droplets spread on (c) the PCL core-spun yarn and (d) the 1DTAB/PCL core-spun yarn. Cross-sectional fluorescence images of the (e) PCL core-spun yarn and (f) 1DTAB/PCL core-spun yarn. (g) The OMMC and R values of the tree-like core-spun yarn-based fabrics.

extremely small (Figure 4e,f), the capillary pressure within the nanofiber layer should be sharply strengthened. As a result, although water could enter into the fabric easily, it would be trapped in the nanofiber layer; thus, the WCB increased slowly. To observe this process in a more visual manner, a water droplet (4 °C, 200 μL) was dropped onto the fabric samples (2 × 2 cm), and an IR thermal imager recorded the motion process of the liquid flow. The test images acquired at 30 s are presented in Figure 4g, and they validly confirmed the results of the MMT. For the PCL fabric and 0.25DTAB/PCL fabric (Movies S1 and S2), the water droplets could hardly spread on their top surface and instead maintained a ball shape only. Analysis of the 0.5DTAB/PCL fabric and 1DTAB/PCL fabric showed fast water transfer along the tree-like yarns (the weft direction), which was demonstrated in Movies S3 and S4. However, in contrast to that in the 0.5DTAB/PCL fabric, the liquid flow in the 1DTAB/PCL fabric was more inclined to move along the tree-like yarns because the differential capillary effect was strengthened by the enhanced surface wettability of the nanofibers. With a further increase in wettability, this phenomenon became more apparent in the 2DTAB/PCL fabric and 3DTAB/PCL fabric (Movies S5 and S6), on which water could spread in only the weft direction (along the tree-like core-spun yarns). This behavior explains why the water content on the top surface increased rapidly but it was difficult for the water to permeate to the bottom surface. The water transfer performance was further characterized by wicking height test results (Figure S3). For the PCL fabric and 0.25DTAB/PCL fabric, the wicking height along the tree-like yarns was extremely low because of the poor surface wettability and negative capillary pressure. As the concentration of DTAB increased, the wicking height increased, and the 3DTAB/PCL fabric achieved the largest wicking height of 13.4 cm. A water evaporation rate test was also carried out, as shown in Figure S4. Compared to the 2DTAB/PCL fabric and 3DTAB/PCL fabric, the 0.5DTAB/PCL fabric and 1DTAB/PCL fabric had a relatively faster evaporation rate since water was in the nanofiber layer because of the excessively high surface wettability.[14] It should be noted that because the PCL fabric and 0.25DTAB/PCL fabric could not be wetted completely by 0.2 g of deionized water, the water evaporation rate was not tested.

3.4. Mathematic Simulation of Liquid Flow in the Tree-Like Yarn-Based Fabrics. A mathematical model was derived to determine the relation between the liquid flow state and fiber wettability (Figure 5a,b). This model was in accordance with the extension of Hagen–Poiseuille's law to the pressure loss of liquid flow in a fine tube, assuming that the capillary in the fiber assemblies was in the shape of a cylinder. The flow velocity was a function of the pressure difference (ΔP), tube length (L), dynamic viscosity of the liquid (μ), and tube radius (r). It can be expressed as $\overline{v} = \frac{\Delta P}{8\mu L}R^2$, where ΔP denotes the pressure difference produced by the differential capillary effect, which can be described by eq 2

$$\Delta P = P_1 - P_2 = 2\gamma\left(\frac{\cos\theta_1}{\overline{r}_1} - \frac{\cos\theta_2}{\overline{r}_2}\right) \tag{2}$$

where γ is liquid surface tension (which is 0.072 N/m for water); θ_1 and θ_2 are the contact angles of capillaries 1 and 2, respectively, and $\overline{r}_1$ and $\overline{r}_2$ are the capillary equivalent radii of capillaries 1 and 2, respectively. The capillary equivalent radius can be calculated as ,$\overline{r} = r_f\sqrt{\frac{1-V_f}{V_f}}$ [41] where V_f is the fiber

DOI: 10.1021/acsami.9b14370
ACS Appl. Mater. Interfaces 2019, 11, 44682−44690

volume fraction and r_f is the fiber radius. According to the measurement, the V_f values of the PCL nanofiber yarn and the cotton yarn are nearly 11 and 57%, respectively.

Figure 5a,b presents color plots of the liquid flow distance as a function of the contact angle of the nanofibers and the flow velocity. Based on this model, when the contact angle of the nanofibers $\theta_1 > 90°$, the distance of flow decreased with increasing θ. In this case, ΔP was negative, which meant that the direction of ΔP was outward. Therefore, liquid flow should spread in the warp direction (Figure S5a). When $\theta_1 < 90°$, ΔP is positive, and the microfluidic flow should move in the weft direction along the tree-like yarns (Figure S5b). As a result, with the increase in cos θ, the flow distance became longer. From this point of view, the contact angle θ_1 controlled the water motion within the core-spun yarns. Furthermore, to investigate the capillary-driven microfluidics within these core-spun yarn-based fabrics, a mathematical simulation could well fit the results. For the PCL fabric, 0.25DTAB/PCL fabric, and 0.5DTAB/PCL fabric (Figure S6), the water flow mainly spread along the warp direction with flow distances of approximately 6.4, 5.2, and 4.8 cm, respectively. As shown in Figure 5c, the corresponding flow velocities measured by the MMT were approximately 4.5, 3.4, and 2.5 mm/s, respectively. The subsequent decrease in cos θ_1 in the 1DTAB/PCL fabric, 2DTAB/PCL fabric, and 3DTAB/PCL fabric strengthened the microfluidic flow along the core-spun yarns (Figure 5d). The flow distance increased from 4.8 to 6 cm, and the velocity accelerated from 1.9 to 3.9 mm/s (Supporting Information note). On the basis of this mathematical model, the water flow spreading in the fabric could be quantitatively controlled.

The moisture-wicking function of the fabrics was enhanced by controlling the surface wettability of the PCL nanofibers. As shown in Figure 6a and Movie S7, water droplets (50 μL) cannot penetrate into the PCL core-spun yarn-based fabric, as they merely remain as hemispheres on the top surface of the fabric. By contrast, for the 1DTAB/PCL core-spun yarn-based fabric, water droplets not only quickly spread on the top surface but also were rapidly transported to the bottom surface (Figure 6b and Movie S8), indicating enhanced moisture-wicking ability. According to the theory of liquid wicking, these phenomena result from the relationship between hydrostatic pressure and capillary force within tree-like yarns.[42,43] In PCL core-spun yarns, the nanofibers are hydrophobic, so the hydrostatic pressure and capillary force in the nanofiber layer are opposite (Figure S7a). By contrast, in the 1DTAB/PCL core-spun yarns, the hydrostatic pressure and capillary force were in the same direction; thus, water could be continuously transferred to the outer layer (Figure S7b). This mechanism was further confirmed by the water droplet test on a single yarn (Figure 6c,d). Owing to the low surface energy, the water droplet on the PCL core-spun yarn could not be transferred, and it maintained its ball shape on the yarn surface, while the water droplet on the 1DTAB/PCL core-spun yarn with high surface energy could rapidly spread. To observe the water transport behavior within the yarn, fluorescence microscopy was used to evaluate water movement in the cross-section (Figure 6e,f). The PCL and 1DTAB/PCL core-spun yarns were prewetted in deionized water, where eosin Y (water soluble) was added as a tracer dye to detect the water distribution. Compared with that of the PCL core-spun yarn, the wetted region (in green) of the 1DTAB/PCL core-spun yarn was obviously limited to the outer layer, indicating an enhanced moisture-wicking function. Surprisingly, the core layer was still in the nonwetted region (the dark area), which meant that water did not permeate throughout the whole yarn and instead rapidly transferred only through the interface between the inner and outer layers. The cotton fibers could not absorb liquid moisture and were maintained in a dry state. In this situation, water that was transported through the outer layer could be evaporated quickly into the air environment, achieving an outstanding moisture-wicking function. As shown in Figure 6g, the 1DTAB/PCL core-spun yarn-based fabric not only showed an ultrahigh R value (1025%) but also achieved a high overall moisture management capability (OMMC) (0.88), which was two times higher than that of conventional cotton[44] and polyester knitted fabrics[45] and comparable to that of composite fibrous membranes.[46,47] These 1D fiber assemblies have enormous potential in the areas of microfluidic flow,[34−36] functional textiles,[48,49] oil−water separation,[22,50] and fog harvesting.[27,51]

4. CONCLUSIONS

In summary, we emulated a tree-like system with novel electrospinning technology to prepare 1D fiber assemblies by combining structural design and surface wettability control. A tree-like structure with hierarchical multibranch channels was constructed by an electrospun yarn method, and the surface wettability of the nanofibers, which played a dominant role in their water transport behavior, was precisely regulated (CA ranged from 135° to 22°) by adding DTAB. Differential capillary pressure produced by the fiber scale difference could readily pull water into the yarn and transport it rapidly between the sheath and core layers. Furthermore, the surface energy of the nanofibers was optimized to achieve the ability to move water from the top surface to the bottom surface. As a result, among the yarns considered in this work, the 1DTAB/PCL yarns obtained the best water transport property, and fabrics woven from these yarns exhibited relatively high water transport performance (R = 1034.5%, OMMC = 0.88), comparable to that of hierarchical fibrous membranes. Finally, a mathematical model of water moving through the fabric was simulated, thereby confirming that the microfluidic flow within the fabric, based on the differential capillary effect, could be accurately controlled. As expected, this work provided a new strategy for realizing a controllable moisture-wicking function in 1D fiber assemblies.

■ ASSOCIATED CONTENT

Supporting Information

The Supporting Information is available free of charge on the ACS Publications website at DOI: 10.1021/acsami.9b14370.

Schematic diagrams of the tree-like yarn technology and practical process of preparation for tree-like yarns; fiber diameter distribution; wicking height test results; water evaporation rate; the direction of ΔP in the fabric; water transport behaviors of core-spun yarn-based fabrics; hydrostatic pressure and capillary force within core-spun yarns; and supporting note: simulation calculation of relation between flow velocity and contact angles. (PDF)

IR thermal recording for water movement on the PCL tree- like core-spun yarn-based fabrics (AVI)

IR thermal recording for water movement on the 0.25DTAB/PCL tree- like core-spun yarn-based fabrics (AVI)

DOI: 10.1021/acsami.9b14370
ACS Appl. Mater. Interfaces 2019, 11, 44682−44690

IR thermal recording for water movement on the 0.5DTAB/PCL tree- like core-spun yarn-based fabrics (AVI)

IR thermal recording for water movement on the 1DTAB/PCL tree- like core-spun yarn-based fabrics (AVI)

IR thermal recording for water movement on the 2DTAB/PCL tree- like core-spun yarn-based fabrics (AVI)

IR thermal recording for water movement on the 3DTAB/PCL tree- like core-spun yarn-based fabrics (AVI)

Water penetration behavior of the PCL tree-like core-spun yarn-based fabrics (AVI)

Water penetration behavior of the 1DTAB/PCL tree-like core-spun yarn-based fabrics (AVI)

■ AUTHOR INFORMATION

Corresponding Author

*E-mail: xhqin@dhu.edu.cn.

ORCID

Dequn Wu: 0000-0002-1118-8729

Xiaohong Qin: 0000-0003-4663-903X

Notes

The authors declare no competing financial interest.

■ ACKNOWLEDGMENTS

This work was partly supported by the Chang Jiang Youth Scholars Program of China and grants (51773037) from the National Natural Science Foundation of China to X.Q. as well as the "Innovation Program of Shanghai Municipal Education Commission", "Fundamental Research Funds for the Central Universities", and "DHU Distinguished Young Professor Program" to her. This work has also been supported by grant (51803023, 61771123) from the National Natural Science Foundation of China to H.Z. and R.W. and the Shanghai Sailing Program (18YF 1400400), the Project funded by China Postdoctoral Science Foundation (2018M640317) and the Fundamental Research Funds for the Central Universities (2232018A3-11) to Z.Q. and the Graduate Student Innovation Fund of Donghua University (CUSF-DH-D-2019040) to N.M.

■ REFERENCES

(1) Bejan, A. *Shape and Structure, from Engineering to Nature [M]*; Cambridge University Press, 2000.

(2) Martinez, A. W.; Phillips, S. T.; Whitesides, G. M.; Carrilho, E. Diagnostics for the Developing World: Microfluidic Paper-Based Analytical Devices. *Anal. Chem.* **2010**, *82*, 3−10.

(3) Ma, M.; Guo, L.; Anderson, D. G.; Langer, R. Bio-Inspired Polymer Composite Actuator and Generator Driven by Water Gradients. *Science* **2013**, *339*, 186−189.

(4) Bai, H.; Ju, J.; Zheng, Y.; Jiang, L. Functional Fibers with Unique Wettability Inspired by Spider Silks. *Adv. Mater.* **2012**, *24*, 2786−2791.

(5) Wheeler, T. D.; Stroock, A. D. The transpiration of water at negative pressures in a synthetic tree. *Nature* **2008**, *455*, 208−212.

(6) Fan, J. T.; Sarkar, M. K.; Szeto, Y. C.; Tao, X. M. Plant structured textile fabrics. *Mater. Lett.* **2007**, *61*, 561−565.

(7) Fan, J.; Cheng, Q.; Zhao, L.-Y.; Liu, Y.; Ma, C.-Q. A BIOMIMIC THERMAL FABRIC WITH HIGH MOISTURE PERMEABILITY. *Therm. Sci.* **2013**, *17*, 1425−1430.

(8) Zhao, Y.; Wang, H.; Zhou, H.; Lin, T. Directional Fluid Transport in Thin Porous Materials and its Functional Applications. *Small* **2017**, *13* (), DOI: 10.1002/smll.201601070. DOI: 10.1002/smll.201770020

(9) Aizenberg, J.; Weaver, J. C.; Thanawala, M. S.; Sundar, V. C.; Morse, D. E.; Fratzl, P. Skeleton of Euplectella sp.: Structural hierarchy from the nanoscale to the macroscale. *Science* **2005**, *309*, 275−278.

(10) Liu, K.; Jiang, L. Bio-inspired design of multiscale structures for function integration. *Nano Today* **2011**, *6*, 155−175.

(11) Zheng, X.; Shen, G.; Wang, C.; Li, Y.; Dunphy, D.; Hasan, T.; Brinker, C. J.; Su, B.-L. Bio-inspired Murray materials for mass transfer and activity. *Nat. Commun.* **2017**, *8*, 14921.

(12) Wang, Z.; Liu, T.; Yu, Y.; Asif, M.; Xu, N.; Xiao, F.; Liu, H. Coffee Ring-Inspired Approach toward Oriented Self-Assembly of Biomimetic Murray MOFs as Sweat Biosensor. *Small* **2018**, *14* (), 1802670, DOI: 10.1002/smll.201802670. DOI: 10.1002/smll.201802670

(13) Guo, T.; Che, P.; Heng, L.; Fan, L.; Jiang, L. Anisotropic Slippery Surfaces: Electric-Driven Smart Control of a Drop's Slide. *Adv. Mater.* **2016**, *28*, 6999−7007.

(14) Miao, D.; Huang, Z.; Wang, X.; Yu, J.; Ding, B. Continuous, Spontaneous, and Directional Water Transport in the Trilayered Fibrous Membranes for Functional Moisture Wicking Textiles. *Small* **2018**, No. e1801527.

(15) Murray, C. D. The Physiological Principle of Minimum Work: I. The Vascular System and the Cost of Blood Volume. *Proc. Natl. Acad. Sci. U.S.A.* **1926**, *12*, 207−214.

(16) Sherman, T. F. On connecting large vessels to small. The meaning of Murray's law. *J. Gen. Physiol.* **1981**, *78*, 431−453.

(17) Shan, X. D.; Wang, M.; Guo, Z. Y. Geometry Optimization of Self-Similar Transport Network. *Math. Probl. Eng.* **2011**, *2011*, 1−11.

(18) Bejan, A.; Lorente, S. Constructal law of design and evolution: Physics, biology, technology, and society. *J. Appl. Phys.* **2013**, *113*, 151301.

(19) Wang, Z.; Wang, Y.; Liu, G. Rapid and Efficient Separation of Oil from Oil-in-Water Emulsions Using a Janus Cotton Fabric. *Angew. Chem. Int. Ed.* **2016**, *55*, 1291−1294.

(20) Wang, H.; Ding, J.; Dai, L.; Wang, X.; Lin, T. Directional water-transfer through fabrics induced by asymmetric wettability. *J. Mater. Chem.* **2010**, *20*, 7938−7940.

(21) Wang, H.; Zhou, H.; Yang, W.; Zhao, Y.; Fang, J.; Lin, T. Selective, Spontaneous One-Way Oil-Transport Fabrics and Their Novel Use for Gauging Liquid Surface Tension. *ACS Appl. Mater. Interfaces* **2015**, *7*, 22874−22880.

(22) Tian, X.; Jin, H.; Sainio, J.; Ras, R. H. A.; Ikkala, O. Droplet and Fluid Gating by Biomimetic Janus Membranes. *Adv. Funct. Mater.* **2014**, *24*, 6023−6028.

(23) Zeng, C.; Wang, H. X.; Zhou, H.; Lin, T. Directional Water Transport Fabrics with Durable Ultra-High One-Way Transport Capacity. *Adv. Mater. Interfaces* **2016**, *3*, 1600036.

(24) Wu, J.; Wang, N.; Wang, L.; Dong, H.; Zhao, Y.; Jiang, L. Unidirectional water-penetration composite fibrous film via electrospinning. *Soft Matter* **2012**, *8*, 5996−5999.

(25) Dong, Y.; Kong, J.; Phua, S. L.; Zhao, C.; Thomas, N. L.; Lu, X. Tailoring Surface Hydrophilicity of Porous Electrospun Nanofibers to Enhance Capillary and Push-Pull Effects for Moisture Wicking. *ACS Appl. Mater. Interfaces* **2014**, *6*, 14087−14095.

(26) Tian, X.; Li, J.; Wang, X. Anisotropic liquid penetration arising from a cross-sectional wettability gradient. *Soft Matter* **2012**, *8*, 2633−2637.

(27) Cao, M.; Xiao, J.; Yu, C.; Li, K.; Jiang, L. Hydrophobic/Hydrophilic Cooperative Janus System for Enhancement of Fog Collection. *Small* **2015**, *11*, 4379−4384.

(28) Wang, X.; Huang, Z.; Miao, D.; Zhao, J.; Yu, J.; Ding, B. Biomimetic Fibrous Murray Membranes with Ultrafast Water Transport and Evaporation for Smart Moisture-Wicking Fabrics. *ACS Nano* **2018**, *13*, 1060−1070.

(29) Ravandi, S. A. H.; Sanatgar, R. H.; Dabirian, F. Wicking Phenomenon in Nanofiber-Coated Filament Yarns. *J. Eng. Fibers Fabr.* **2013**, *8*, 10−18.
(30) Rahbar, R. S.; Maleki, H.; Kalantari, B. Fabrication of electrospun nanofibre yarn based on nylon 6/microencapsulated phase change materials. *J. Exp. Nanosci.* **2016**, *11*, 1402−1415.
(31) Wu, S.-H.; Qin, X.-H. Uniaxially aligned polyacrylonitrile nanofiber yarns prepared by a novel modified electrospinning method. *Mater. Lett.* **2013**, *106*, 204−207.
(32) Zhou, Y.; He, J.; Wang, H.; Qi, K.; Ding, B.; Cui, S. Carbon nanofiber yarns fabricated from co-electrospun nanofibers. *Mater. Des.* **2016**, *95*, 591−598.
(33) Sajadifar, S. A.; Karimipour, A.; Toghraie, D. Fluid flow and heat transfer of non-Newtonian nanofluid in a microtube considering slip velocity and temperature jump boundary conditions. *Eur. J. Mech. B Fluid* **2017**, *61*, 25−32.
(34) Shou, D.; Fan, J. Design of Nanofibrous and Microfibrous Channels for Fast Capillary Flow. *Langmuir* **2018**, *34*, 1235−1241.
(35) Liu, M.; Wu, J.; Gan, Y.; Hanaor, D. A. H.; Chen, C. Q. Evaporation Limited Radial Capillary Penetration in Porous Media. *Langmuir* **2016**, *32*, 9899−9904.
(36) Nilghaz, A.; Ballerini, D. R.; Shen, W. Exploration of microfluidic devices based on multi-filament threads and textiles: A review. *Biomicrofluidics* **2013**, *7*, 051501.
(37) Wu, S.; Duan, B.; Qin, X.; Butcher, J. T. Nanofiber-structured hydrogel yarns with pH-response capacity and cardiomyocyte-drivability for bio-microactuator application. *Acta Biomater.* **2017**, *60*, 144−153.
(38) Wu, S.; Liu, P.; Zhang, Y.; Zhang, H.; Qin, X. Flexible and conductive nanofiber-structured single yarn sensor for smart wearable devices. *Sens. Actuators, B* **2017**, *252*, 697−705.
(39) Hammond, P. T. *Colloids and Colloid Assemblies: Synthesis, Modification, Organization and Utilization of Colloid Particles*; Caruso, F., Ed.; Wiley: Weinheim, Germany, 2003; pp. 317−341.
(40) Chen, F.; Lee, C. N.; Teoh, S. H. Nanofibrous modification on ultra-thin poly(epsilon-caprolactone) membrane via electrospinning. *Mater. Sci. Eng., C* **2007**, *27*, 325−332.
(41) Fang, L.; Jiang, J.; Wang, J.; Deng, C. Non-uniform capillary model for unidirectional fiber bundles considering pore size distribution. *J. Reinf. Plast. Compos.* **2014**, *33*, 1430−1440.
(42) Guo, T.; Han, K.; Heng, L.; Cao, M.; Jiang, L. Ordered porous structure hybrid films generated by breath figures for directional water penetration. *RSC Adv.* **2015**, *5*, 88471−88476.
(43) Heng, L.; Liu, J.; Hu, R.; Han, K.-Y.; Guo, L.-L.; Liu, Y.; Li, M.-Y.; Nie, Q. Wettability and permeation of ethanol/water mixture on porous mesh surface. *RSC Adv.* **2016**, *6*, 77340−77345.
(44) Danino, D.; Marmur, A. Radial Capillary Penetration Into Paper—Limited And Unlimited Liquid Reservoirs. *J. Colloid Interface Sci.* **1994**, *166*, 245−250.
(45) Kwok, D. Y.; Budziak, C. J.; Neumann, A. W. Measurements Of Static And Low-Rate Dynamic Contact Angles By Means Of An Automated Capillary Rise Technique. *J. Colloid Interface Sci.* **1995**, *173*, 143−150.
(46) Ahmad, I.; Kan, C.-w. A Review on Development and Applications of Bio-Inspired Superhydrophobic Textiles. *Materials* **2016**, *9*, 892.
(47) Babar, A. A.; Miao, D.; Ali, N.; Zhao, J.; Wang, X.; Yu, J.; Ding, B. Breathable and Colorful Cellulose Acetate-Based Nanofibrous Membranes for Directional Moisture Transport. *ACS Appl. Mater. Interfaces* **2018**, *10*, 22866−22875.
(48) Sarkar, M.; Jintu Fan, J. T.; Szeto, Y.-c.; Xiaoming Tao, X. M. Biomimetics of Plant Structure in Textile Fabrics for the Improvement of Water Transport Properties. *Text. Res. J.* **2009**, *79*, 657−668.
(49) Nazir, A.; Hussain, T.; Abbas, G.; Ahmed, A. Effect of Design and Method of Creating Wicking Channels on Moisture Management and Air Permeability of Cotton Fabrics. *J. Nat. Fibers* **2015**, *12*, 232−242.
(50) Zhou, X.; Zhang, Z.; Xu, X.; Guo, F.; Zhu, X.; Men, X.; Ge, B. Robust and Durable Superhydrophobic Cotton Fabrics for Oil/Water Separation. *ACS Appl. Mater. Interfaces* **2013**, *5*, 7208−7214.
(51) Garrod, R. P.; Harris, L. G.; Schofield, W. C. E.; McGettrick, J.; Ward, L. J.; Teare, D. O. H.; Badyal, J. P. S. Mimicking a stenocara beetle's back for microcondensation using plasmachemical patterned superhydrophobic-superhydrophilic surfaces. *Langmuir* **2007**, *23*, 689−693.

DOI: 10.1021/acsami.9b14370
ACS Appl. Mater. Interfaces 2019, 11, 44682−44690